KURENAI
Kyoto University Research Information Repository

KYOTO UNIVERSITY

Title	A New Electrolytic Production Process of Silicon Using Liquid Zn Alloy Cathode in Molten Salt
Author(s)	Nohira, Toshiyuki; Ido, Akifumi; Shimao, Takeyuki; Yang, Xiao; Yasuda, Kouji; Homma, Takayuki; Hagiwara, Rika
Citation	ECS Transactions (2016), 75(15): 17-33
Issue Date	2016
URL	http://hdl.handle.net/2433/236052
Right	
Type	Conference Paper
Textversion	author

Kyoto University

A New Electrolytic Production Process of Silicon Using Liquid Zn Alloy Cathode in Molten Salt

Toshiyuki Nohira[a], Akifumi Ido[b], Takeyuki Shimao[b], Xiao Yang[a],
Kouji Yasuda[b,c], Rika Hagiwara[a] and Takayuki Homma[d]

[a] Institute of Advanced Energy, Kyoto University, Uji 611-0011, Japan.
[b] Graduate School of Energy Science, Kyoto University, Kyoto 606-8501, Japan
[c] Environment, Safety and Health Organization, Kyoto University,
Kyoto 606-8501, Japan
[d] Faculty of Science and Engineering, Waseda University,
Tokyo 169-8555, Japan.

Electrolytic production process for solar-grade Si utilizing liquid Si–Zn alloy cathode in molten $CaCl_2$ has been proposed. Toward the establishment of the process, the behavior of liquid Zn metal was investigated in molten $CaCl_2$ at 1123 K. The evaporation of Zn metal was largely suppressed by an immersion into molten salt, which enables the use of Zn electrode in spite of the high vapor pressure of Zn. The cyclic voltammetry suggested the reduction of SiO_2 at 1.45 V vs. Ca^{2+}/Ca on a Zn cathode. After the potentiostatic electrolysis at 0.9 V, Si particles with diameters of 2–30 µm were precipitated in the solidified Zn matrix by the slow cooling process of the produced liquid Si–Zn alloy. The alloying rate between solid Si and liquid Zn was measured as 4.56 µm s^{-1}, and it linearly decreased with the Si content in liquid Zn phase.

Introduction

Photovoltaic (PV) power generation has been developed as one of the key technologies that can mitigate the energy and environmental issues. For examples, there were several national projects in 1970s such as Sunshine Project by Ministry of International Trade and Industry (MITI) in Japan and Federal Photovoltaic Utilization Program by Department of Energy (DOE) in the United States. Since then, the situation has drastically changed in this decade; the increased installation of the PV cells promoted by the political and financial supports in various countries, the broadened usage from the conventional electronic calculator and independent power source to the large scale power station, and the diversification of the solar cell materials. Accordingly, the production volume of PV cells has increased in 21st century by a factor of more than 100; 285 MW in 2000 and 36,100 MW in 2013 [1]. Non-silicon materials occupied only 0.4% of the production volume of solar cells in 2000, and reached 7.6% in 2013 because of the compound-type solar cells such as CdTe type and Cu-In-Ga-Se (CIGS) type [1].

As a matter of course, the PV cell installation will increase more and more in the future as one of the key technologies for environmental issues and diversification of energy source. In the light of the solar cell materials, compound-type solar cells have drawbacks for mass production because the production capacities are limited by the supply of the component materials obtained as byproducts in nonferrous metallurgy. For instance, the production capacity of CdTe solar cells are at most 6 to 8 GW per year

owing to the supply capacity of Te [2], and 20 to 30 GW for CIGS solar cells. Therefore, crystalline Si solar cells are most likely to be continuously a main stream of the PV industry in the long run.

High-purity Si used for crystalline Si solar cells are called as a solar-grade Si (SOG-Si), which exceeds the purity of 5N-7N. Siemens process [3–6] utilizing H_2 reduction and/or thermal decomposition of trichlorosilane ($SiHCl_3$), which is the current production process of SOG-Si, was originally developed for a manufacture of a semiconductor-grade Si (SEG-Si, 11N–12N purity) for large scale integrated circuits (LSIs). Due to the reaction kinetics of silane gases, Siemens process has inherent drawbacks of low productivity and low energy efficiency. To develop a next generation production process of SOG-Si, various types of production or refining processes of Si, which can overcome the low productivity of the conventional Siemens process, have been investigated: H_2 reduction and/or decomposition of silane-based gases in improved Siemens-based processes, metallothermic reduction of silicon halides by metal reductants such as zinc and aluminum, and purification of metallurgical-grade Si (MG-Si; 98‑99% purity) using metallurgical purification methods [7,8]. Recently, the fluidized bed reaction (FBR) of monosilane (SiH_4) in REC Silicon and SunEdison Samsung Fine Chemicals, and upgrading metallurgical-grade Si (UMG) using various refining techniques have been operated in a mass scale [9].

In our group, the direct electrolytic reduction of solid SiO_2 to Si has been studied in molten $CaCl_2$ at 1123 K as a new type of electrochemical reaction [10–12]. In this method, electrochemical reduction of insulating SiO_2 proceeds by the use of a SiO_2 contacting electrode which gives a three-phase interface between conductor/SiO_2/molten salt.

$$SiO_2 \text{ (s)} + 4 \text{ e}^- \text{ (through conductor)} \rightarrow Si \text{ (s)} + 2 \text{ O}^{2-} \tag{1}$$

We also proposed that the combination of the electrolytic reduction of purified SiO_2 and a directional solidification refinement is a potential method to realize the low-cost production of SOG-Si [13,14]. Recently, in order to improve the productivity of the process, we have studied the electrochemical reduction of SiO_2 granules set on the bottom cathode in molten $CaCl_2$ on the analogy of the Hall-Héroult Al production process [15]. By many research groups including us, the direct electrochemical reduction of SiO_2 has been widely investigated for SOG-Si production [16–34]. However, the recovery of the powdery Si product from mixture of Si, SiO_2 and $CaCl_2$ is one of challenges. Since the separation between solid product and molten salt is an inherent problem for molten salt processes, the cathodic products are usually manufactured in the liquid state for the easiness of the subsequent recovery in the practical production processes of Li, Na, Mg, and Al metal, and rare earth alloys. Thus, we expected that a utilization of liquid Si alloy cathode would be a solution for the SOG-Si production process in molten $CaCl_2$.

A typical recovery method of a certain metal from liquid alloy utilizes the principle of a solubility decrease upon temperature lowering. A well-known industrial process is the simultaneous metallurgical production of Zn and Pb called as the Imperial Smelting Process (ISP). When the liquid Si alloy cathode is applicable to the electrolytic reduction of SiO_2 in molten salt, there are many advantages such as the easy separation of Si from molten salt and unreacted SiO_2, and the easy transfer from the electrolysis cell. Further, since metallurgical-grade Si can be refined by a solidification of liquid Si alloys [35–49],

high separation ability is expected in the Si precipitation process from liquid alloy, in which impurities are enriched in the liquid phase.

As an alloying element for Si which gives liquid alloy, Zn, Sn, Pb, and Al are candidates because they have no intermetallic compounds with Si. Their characters are summarized in Table 1 [50–57]. Although Al looks promising due to the larger solubility at the electrolysis temperature, the removal of Al soluted in Si phase is difficult even to 100 ppm, which were reported in the electrolysis of SiO_2 on Al cathode [28] and the refining of low-purity Si utilizing Si–Al alloy [35–39]. Considering many factors, we selected Zn as an alloying element because the lower boiling point and smaller distribution coefficients are advantageous for obtaining high-purity Si products after vacuum refining and directional solidification in the final step.

Table 1 Properties of alloying elements for Si.

Metal	$T_{m.p.}$ / K	$T_{b.p.}$ / K	Solubility of Si at 1123 K / mol%	Distribution coefficient at $T_{m.p.}$ (Si)
Zn	693 [48]	1180 [48]	6.0 [52]	1×10^{-5} [52]
Sn	505 [51]	2875 [51]	0.9 [53]	1.6×10^{-2} [53]
Pb	601 [48]	2019 [48]	< 0.2 [54]	2×10^{-3} [56]
Al	933 [48]	2791 [48]	32.6 [55]	2×10^{-3} [57]

Figure 1 shows a schematic illustration of the proposed process for SOG-Si production utilizing a liquid Si–Zn alloy cathode in molten salt. The overall process is composed of three major processes: an electrolysis process, a precipitation process, and a refining process. In the electrolysis process, solid SiO_2 is reduced to form Si–Zn liquid alloy on the cathode.

$$SiO_2 \text{ (s)} + \text{Si–Zn } (l, \text{ low Si conc.}) + 4e^- \rightarrow \text{Si–Zn } (l, \text{ high Si conc.}) + 2O^{2-} \qquad (2)$$
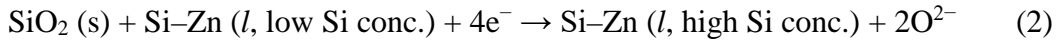
Figure 2(a) and 2(b) shows the whole range and Zn-rich side of the phase diagram for the Si–Zn system [52], respectively. Here, the temperature and composition changes in the proposed process are indicated in Fig. 2(b) with the arrows. The solubility of Si in liquid Zn is 6 at% at 1123 K. The Si–Zn liquid alloy produced at the bottom of the electrolysis cell is separated from the molten salt due to the density difference, and is transferred to the precipitation process. In the precipitation process, metallic Si is recovered by lowering the temperature.

$$\text{Si–Zn } (l, \text{ high Si conc.}) \rightarrow \text{Si (s)} + \text{Si–Zn } (l, \text{ low Si conc.}) \qquad (3)$$
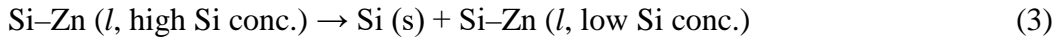
When the temperature is lowered to 923 K, the solubility is also lowered to 1 at%-Si, thus, solid Si of 5 at% with reference to Zn is recovered. After the precipitation process, the Si–Zn alloy with low Si concentration is reused as the cathode in the electrolysis process. The produced Si is further transferred to the refining process. An ingot of SOG-Si is manufactured by a directional solidification of the Si treated after leaching and vacuum refining.

This process is expected to have several advantages in terms of productivity and purification ability. In contrast to the Siemens process, the proposed process can be

operated semi-continuously, which contributes to the high productivity. High purification efficiency is expected in the two-times segregation step; the deposition of solid Si from Si–Zn liquid alloy in the precipitation, and the precipitation of solid Si from liquid Si in the refining processes. Low distribution coefficients for the impurity elements, which mean the high purification ability, are reported both for the precipitation from liquids of metallic Si [57] and alloys of Si–Al [35–39], Si–Cu [40,41], Si–Sn [42,44], Si–Fe [45–47], Si–Ni [48], and Si–Na [49]. Furthermore, the remaining Zn can be easily removed to several ppms even by the evacuation techniques used more than 30 years ago [58]. More complete removal of Zn is possible by using the advanced vacuum refining technology.
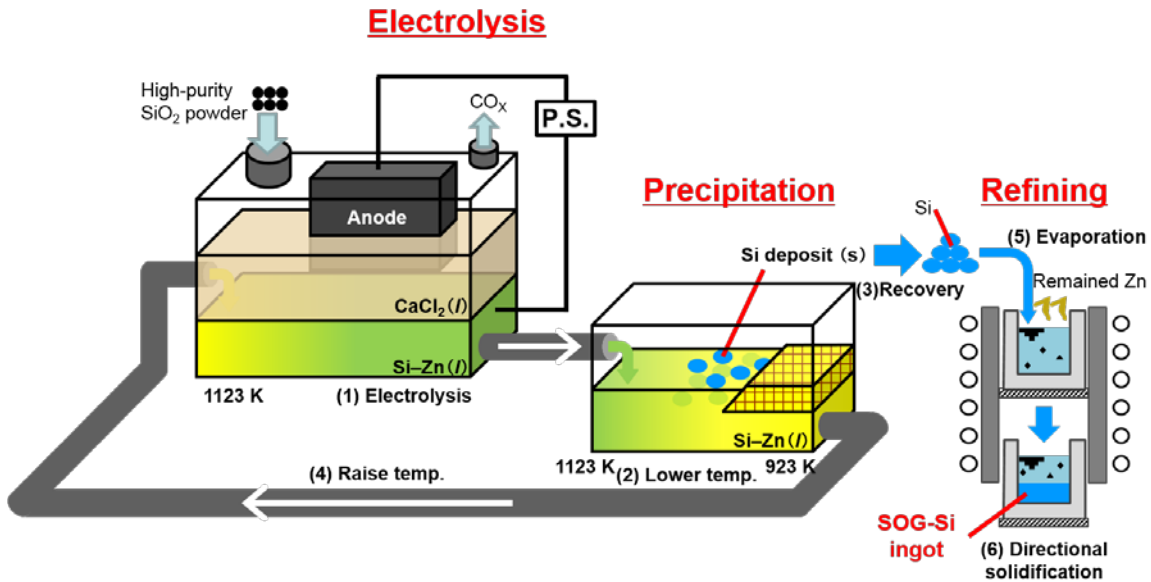

Figure 1. A schematic drawing of solar-grade Si production utilizing an electrochemical reduction of SiO₂ powder on a liquid Si–Zn alloy cathode in molten CaCl₂.
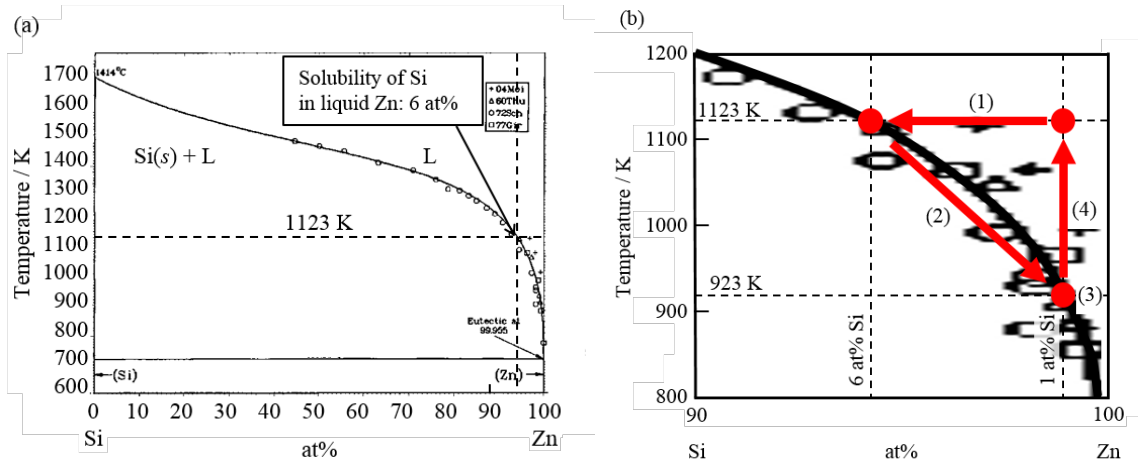

Figure 2. (a) A binary phase diagram for the Si–Zn system [52]. (b) Temperature and alloy composition in the production process.

(1) SiO$_2$ is electrochemically reduced to liquid Si–Zn alloy with Si concentration of 6.0 at% on the bottom cathode.

(2) Liquid 6.0at%Si–Zn alloy is recovered from the bottom of the electrolytic cell, and then cooled to 923 K to precipitate metallic Si corresponding to 5.0 at% with respect to Zn.

(3) Precipitated metallic Si is recovered.

(4) Liquid 1.0at%Si–Zn alloy is heated to 1123 K to reuse as the bottom cathode.

In this study, fundamentals on the electrolysis process, namely, the evaporation of Zn metal in molten $CaCl_2$, the electrochemical reduction of SiO_2 on Zn cathode, and alloying rate for the Si–Zn system, were investigated at 1123 K. The effect of immersion into molten $CaCl_2$ on evaporation behavior of Zn metal was analyzed. Regarding the electrochemical behavior of liquid Zn electrode, Kipouos et al. reported the electrolysis of Ca-Zn liquid alloy in molten $CaCl_2$–CaO–CaF_2 system at 973-1023 K [59]. However, the electrode potential was unclear because the two-electrode system was employed. In the present study, we investigated the effective potential range for the production of Si–Zn alloy in the electrolysis of SiO_2 granules on Zn electrode. Furthermore, the alloying rate was studied to estimate the rate-determining step on the electrochemical reaction on Zn electrode.

Experimental

Evaporation of Zn

The evaporation rate of Zn in an Ar atmosphere at 1123 K was measured by the weight change of Zn metal (Kojundo Chemical Laboratory Co., Ltd., 99.9999%, grains, 5.4~5.6 g) set at the bottom of a silica tube (outer diameter (o.d.); 12.5 mm, inner diameter (i.d.); 10.5 mm) with/without the addition of $CaCl_2$ (Kojundo Chemical Laboratory Co., Ltd., 99% up, 5.4~5.6 g or 8.2~8.4 g). The samples dried under vacuum at 453 K for 24 h were contained in a silica tube in a glove bag under an Ar atmosphere. Then, a balloon was set to the open end of the tube with a paraffin film to maintain the atmosphere. The tube was inserted to a silica chamber (i.d. 127 mm, height 403 mm) in an electric furnace maintained at 1123 K, and was left for a given period of time. The tube was pulled out in one minute, and then cooled at room temperature. The Zn sample was weighed after water washing and drying. In the case that the separation of Zn sample from the silica tube was difficult, its weight was calculated from the values before and after leaching treatment with 1M HCl solutions. The Zn content in the molten salt was analyzed by inductively coupled plasma atomic emission spectrometry (ICP-AES: Thermo Scientific, iCAP 6200 Duo) for a solution prepared by dissolving 0.1 g of recovered $CaCl_2$ into HNO_3 solution.

Electrochemical behavior

Figure 3 shows the schematic illustration of the electrochemical apparatus. 350 g of $CaCl_2$ was charged in an alumina crucible (Nikkato Corp., SSA-S grade, o.d. 87 mm, i.d. 80 mm, height 129 mm) and dried under vacuum at 453 K and 773 K for 24 h, respectively. All the electrochemical experiments were carried out in a dry Ar atmosphere at 1123 K. Electrochemical behavior was investigated by cyclic voltammetry and potentiostatic electrolysis using a newly designed liquid Zn electrode. Figure 4 shows a photograph and a schematic illustration of a liquid Zn electrode. Zn grains (Kojundo Chemical Laboratory Co., Ltd., 99.9999%, grains, 3~5 mm, 1.3 g) were set at the bottom of an alumina tube (Nikkato Corp., SSA-S grade, o.d. 13 mm, i.d. 9 mm) with an open window with a size of 10 mm × 20 mm at the side. A Mo wire (Nilaco Corp., dia. 1.0 mm, 99.95%) thread into an alumina insulating tube (Nikkato Corp., SSA-S grade, o.d. 2.0

mm, i.d. 1.0 mm) was used to an electric lead. Purified SiO_2 grains (Taiheiyo Cement Corp., dia. < 0.1 mm, 0.30 g) was set above the Zn grains. The densities of liquid Zn, solid SiO_2 and molten $CaCl_2$ are 5.9 g cm^{-3} [60], 2.2 g cm^{-3}, 2.05 g cm^{-3} [61] at 1123 K, respectively. The counter electrode was a graphite rod (Tokai Carbon Co., Ltd., dia. 5.0 mm). An Ag^+/Ag electrode was used as a reference electrode [17]. In the cyclic voltammetry, an in-situ IR compensation using the electrochemical measurement system was carried out with a compensation ratio of 95% which was the highest value in the range without bringing potential instability. The sample after potentiostatic electrolysis was recovered from the cell in one minute, followed by cooling at room temperature. The samples contained in the alumina tube were cut into halves, and were polished with emery paper (#240, 400, 600, 1000, and 2000) and buffing compound (Micro Polish II, 0.3 μm, Buehler). The analysis was carried with scanning electron microscopy, (SEM; Keyence Corp., VE-8800) and energy-dispersive X-ray spectroscopy (EDX; AMETEK, EDAX Genesis APEX2).
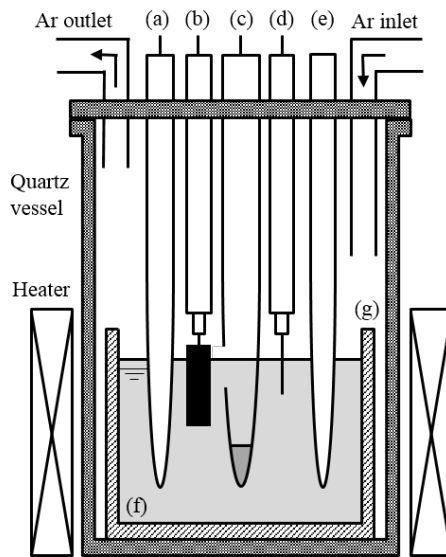

Figure 3. A schematic drawing of the electrolysis cell. (a) Ag^+/Ag reference electrode, (b) graphite counter electrode, (c) liquid Zn electrode with SiO_2 granules, (d) Ca^{2+}/Ca dynamic reference electrode on a Mo wire, (e) thermocouple, (f) molten $CaCl_2$, and (g) alumina crucible.
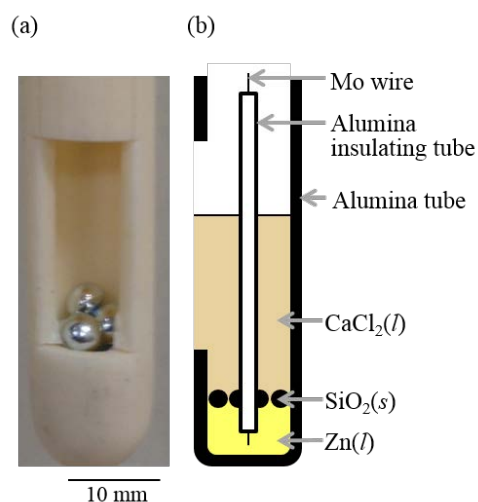
Figure 4. (a) A photograph and (b) schematic illustration of the Zn electrode.

Alloying reaction between solid Si and liquid Zn

330 g or 660 g of Zn granules (Wako Pure Chemical Industries, Ltd., grains) were charged into 210 g of molten $CaCl_2$ to prepare Zn pool in a graphite crucible (Toyo Tanso Co., Ltd., IG-110 grade, o.d. 90 mm, i.d. 80 mm, height 120 mm) in a dry Ar atmosphere at 1123 K. Single crystal Si plates (SUMCO Corp., 6 mm×35 mm, thickness 0.5 mm, n-type, (100) plane, resistivity 1–10 Ω cm) or Si prismatic rods (Furuuchi Chemical Corp., 4 mm×4 mm, height 30 mm) attached to Ni wire (Ryoko Sangyo Co., Ltd. >99%, dia. 1.0 mm) and mullite tubes (Nikkato Corp., HB-grade, o.d. 6 mm, i.d. 4 mm, length 500 mm) were immersed into the Zn pool for 2–60 seconds. Si round rods (Furuuchi Chemical Corp., dia. 6 mm, length 50 mm) fixed to a stainless steel tube (SUS304, o.d. 12.0 mm, i.d. 8.0 mm, length 500 mm) with a ceramic bond was also used for the measurements. For some experiments, Si lumps were added to liquid Zn pool to prepare Si–Zn alloys. Si samples were immersed to the Zn pool or Si–Zn pool for a fixed duration time, and then pulled out to be cooled at room temperature. After washing of the adhered salt with water, the thickness or diameter of the Si specimens before and after the immersion was measured by a micrometer.

Results and discussion

Evaporation of Zn

Prior to the electrochemical experiments, to eliminate the concern that metallic Zn is not utilized as a liquid electrode because of the immediate evaporation at the temperature close to its boiling point; the vapor pressure of Zn at the electrolysis temperature of 1123 K is 0.54 atm [50]. Thus, evaporation behavior of Zn immersed in molten $CaCl_2$ was measured.

Figure 5 shows the photographs before and after the evaporation experiments at 1123 K for 6 h. When only Zn metal was set at the bottom of the tube in Ar atmosphere, a considerable amount of Zn deposits was observed at the upper part of tube inside where the temperature was lower (Fig. 5(a-2)). These deposits result from the evaporation and transport from the liquid Zn in the gas phase. On the other hand, in the presence of molten $CaCl_2$ layer of 5.4–5.6 g, solidified $CaCl_2$ and Zn layers were observed and no

deposit was formed at the upper part as shown in Fig. 5(b-2). The position order of these layers is determined by the density, and the layer thickness is as large as the calculated values (Zn; 10 mm, CaCl$_2$; 31 mm). The weight loss of Zn metal in the experiments with/without the presence of molten CaCl$_2$ over liquid Zn is summarized in Table 2 and plotted in Fig. 6 (a) with reaction time. The graph obviously shows that the evaporation is significantly suppressed by the presence of molten salt above liquid Zn metal. In both cases, the weight of Zn metal almost linearly decreases with time. The evaporation rate determined by the slope of the plot is 1.90×10^{-1} g cm^{-2} h^{-1} when only Zn metal was used. The rate greatly decreased to 4.45×10^{-3} g cm^{-2} h^{-1} (0.023 times) with the presence of molten salt, which corresponds to the evaporation rate of 0.18 mm day^{-1}. Thus, the evaporation of Zn metal covered with molten CaCl$_2$ is found to be negligibly small when it is used as a cathode in the electrolysis process in spite of the high vapor pressure of Zn.

Figure 6(b) compares the evaporation behavior at different thickness of molten CaCl$_2$ layer. The evaporation rates at 31 mm and 47 mm thickness are 4.45×10^{-3} g cm^{-2} h^{-1} and 2.75×10^{-3} g cm^{-2} h^{-1}, respectively. Since the concentration of Zn in molten CaCl$_2$ after the reaction for 24 hours at 31 mm thickness was 0.91wt% determined by ICP-AES, Zn metal is thought to firstly dissolve to the molten salt and then evaporate at the interface between the gas and molten salt after the transport in the melt. As shown in Fig. 6(b), the rate of weight loss varies inversely as layer thickness of CaCl$_2$. Thus, the diffusion in the molten salt is likely the rate determining step.

Table 2 Weight of Zn samples after evaporation experiments at 1123 K.

Time, t / h	Thickness of CaCl$_2$ layer, l_{CaCl_2} / mm	Surface area, A / cm^2	Weight of Zn			
			Before, W_{bef} / g	After, W_{aft} / g	Loss [a], W_{loss} / g	Loss [b], w_{loss} / g cm^{-2}
0.25	0		5.5322	5.2184	3.14×10^{-1}	0.362
0.25	31		5.5119	5.5026	9.30×10^{-3}	0.0107
6	0		5.4502	4.3979	1.05	1.22
6	31	0.866	5.6016	5.5730	2.86×10^{-2}	0.0330
6	47		5.4916	5.4672	2.44×10^{-2}	0.0282
24	0		5.5781	1.6440	3.93	4.54
24	31		5.5310	5.4401	9.09×10^{-2}	0.105
24	47		5.4688	5.4141	5.47×10^{-2}	0.0632

a: $W_{loss} = W_{bef} - W_{aft}$
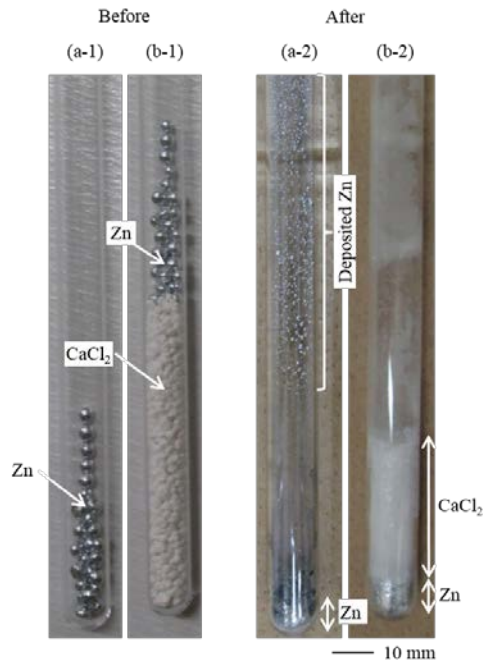b: $w_{loss} = \dfrac{W_{loss}}{A}$

Figure 5 Photographs of the samples before ((a-1) and (b-1)) and after ((a-2) and (b-2)) the evaporation experiments. The evaporation experiments were conducted without ((a-1) and (b-1)) and with ((a-2) and (b-2)) the immersion into molten $CaCl_2$ at 1123 K for 6 h.
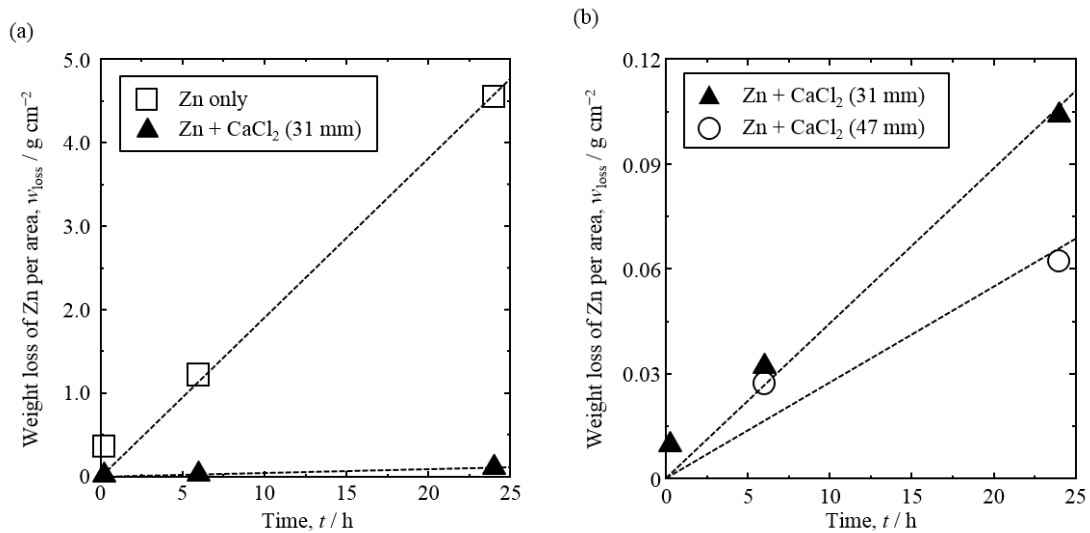

Figure 6. Weight loss of Zn per area at 1123 K. (a) Plots are compared against the immersion of Zn sample in molten $CaCl_2$. (b) Plots are compared against thickness of $CaCl_2$ layer for 31 mm and 47 mm.

Electrochemical behavior

Figure 7 shows the cyclic voltammograms for a liquid Zn electrode with/without SiO_2 granules. The solid curve for Zn metal only indicates the negative current around 50 mA cm^{-2} from the rest potential (1.48 V) and the sharp current increase at 0.9 V. Since Ca and Zn forms a liquid phase over the all composition range at 1123 K [62], this current is supposed to be due to the formation of liquid Ca–Zn alloy. To confirm the reaction, the Zn electrode was galvanostatically electrolyzed at −1.06 A cm^{-2} for 30 min. The open-

circuit potential immediately after the electrolysis was 0.35 V. When the sample was analyzed by EDX, the composition of the surface zone was determined to be 90 at%Zn–10 at%Ca. This value agrees with the calculated value from the reported activity coefficient of Ca in liquid Ca–Zn alloy at 1073 K under Henry's law [63]. Incidentally, Ca content was lower than the detection limit of EDX in the samples obtained by potentiostatic electrolysis at 0.90 V, which is explained by smaller quantity of electricity compared to the galvanostatic electrolysis. From the above results, the reduction current observed at more negative than 0.9 V is attributed to the formation of liquid Ca–Zn alloys.

$$\text{Zn } (l) + y \text{ Ca}^{2+} + 2y \text{ e}^- \rightarrow \text{ZnCa}_y \ (l) \tag{4}$$

The broken curve in Fig. 7 shows the voltammogram for the Zn electrode after the addition of SiO_2. While the rest potential is almost identical before the addition of SiO_2, the larger cathodic currents of 100 mA cm^{-2} are observed during the scan to the negative direction. Thus, the formation of Si–Zn alloy is expected between 0.9 V and 1.45 V. Here, the onset potential of SiO_2 reduction on the liquid Zn cathode (1.45 V) is more positive compared with that on a Mo electrode (1.25 V) [16], which is explained by the lower activity of Si in the Zn-Si alloy.

$$\text{SiO}_2 \ (s) + \text{Zn } (l) + 4\text{e}^- \rightarrow \text{Si–Zn } (l) + 2\text{O}^{2-} \tag{5}$$
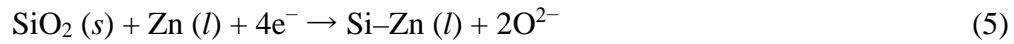
On the basis of the voltammertic results, potentiostatic electrolysis was conducted for a liquid Zn electrode after adding SiO_2 granules with a diameter of 0.1 mm at 0.90 V for 5.5 h in molten $CaCl_2$ at 1123 K. The sample was observed after cross-sectioning in the vertical direction. Figure 8(a) and (b) show cross-sectional optical and SEM images of the sample after the electrolysis, respectively. The precipitated grains are observed only at the upper part of the Zn electrode. As shown in the magnified SEM image in Fig. 8(c) and EDX analysis, Si particles with a diameter of 2~30 µm are deposited in Zn matrix. According to the Si–Zn phase diagram [52], solubility of Si in liquid Zn metal is 6.0 at% at 1123 K and it becomes negligibly small in solid Zn at room temperature. Thus, it is reasonable to conclude that SiO_2 was electrochemically reduced to form liquid Si–Zn alloy (reaction (5)), and that Si particles were precipitated during the cooling process. The Si precipitated particles were observed only at the upper part because they floated and aggregated in the liquid phase due to the smaller density.
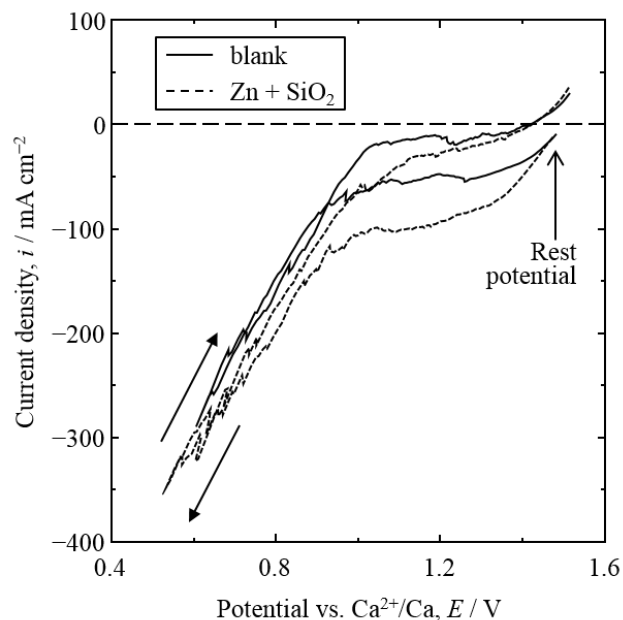
Figure 7. Cyclic voltammograms for liquid Zn electrodes in molten $CaCl_2$ at 1123 K. Scan rate: 0.2 V s^{-1}.
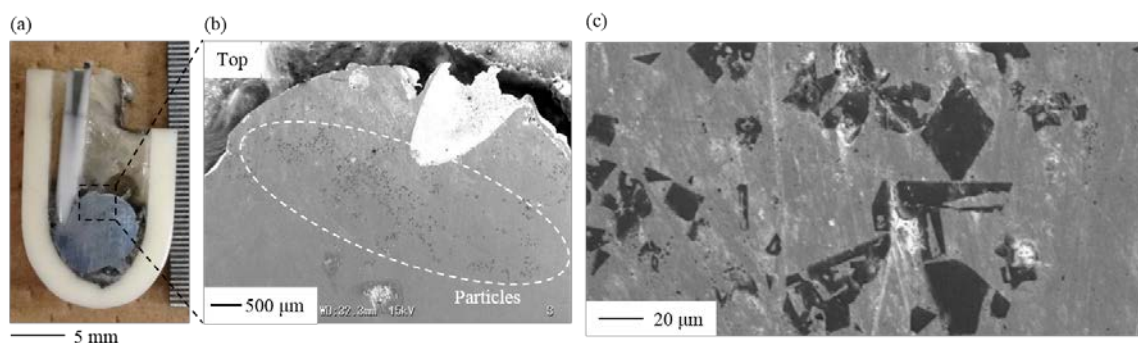

Figure 8. (a) A photograph and (b)(c) cross-sectional SEM images of the sample obtained by potentiostatic electrolysis of liquid Zn electrode with SiO_2 granules at 0.90 V for 60 min in molten $CaCl_2$ at 1123 K.

Alloying reaction between solid Si and liquid Zn

Figure 9 shows the photographs before and after the alloying experiments at 1123 K for different immersion time. After the experiments, Zn was not found on the surface of the recovered Si plate by both direct observation and EDX analysis. The liquid alloy formed at high temperature was probably removed during pulling out through the molten $CaCl_2$ layer. From the photos in Fig. 9, the decrease of plate thickness by the dissolution of Si is clearly observed in direct observation even after the immersion for 2 seconds. For the Si plate reacted for 60 seconds, the whole immersed portion was completely disappeared. Since the alloying reaction proceeds at both the sides of Si plate, the reduced thickness was evaluated as a value for one side, which is listed in Table 3. As shown in Fig. 10, the thickness of the plate linearly decreases with the immersion time, and the alloying rate is determined to be 4.56 µm s^{-1} from the slope of the plots.

The similar measurements were conducted for Si–Zn alloy pools with different Si concentrations, and the results are summarized in Table 3 and Fig. 10. The decrease of alloy formation rate is observed with the Si concentration in liquid alloy. Here, the alloy formation rate (v_{alloy}) is plotted in Fig. 11 against the Si concentration (c_{Si}) in the alloy. Linear relationship between v_{alloy} and c_{Si} is clearly observed.

$$v_{alloy} = -0.747c_{Si} + 4.49 = 0.747\,^*(6.0 - c_{Si}) \tag{6}$$

The extrapolation indicates that alloy formation rate becomes zero at 6.0 at%Si, which agrees with the solubility in liquid Si–Zn alloy [52]. This fact suggests that the alloying reaction is controlled by the diffusion of Si atoms in the diffusion layer between solid Si and liquid Zn. The diffusion of Si in liquid Zn is expected to be fast in the order of 10^{-4} cm^2 s^{-1} from the reported diffusion coefficients, D, of Fe (1–5×10^{-4} cm^2 s^{-1} [64]) and Al (1.1×10^{-4} cm^2 s^{-1} [65]) at 1123 K. From the alloy formation rate of 4.56 µm s^{-1} and the estimated diffusion coefficient of 1×10^{-4} cm^2 s^{-1}, the diffusion layer thickness, l, is calculated to be 145 µm at the reaction time, t', at 1.05 seconds by using the relation of $l = \sqrt{2Dt}$. Thus, the plots in Fig. 10 does not show a parabolic relation but a linear.

In order to estimate the rate-determining step of electrochemical reduction of SiO$_2$ using liquid Zn electrode, the alloying rate is compared with the reaction rate in other steps involved in the reaction. According to our previous studies, the reduction rates are estimated from the results at the reaction time of 300 s in molten CaCl$_2$ at 1123 K as 2.1 µm s^{-1} [18] and 0.27 µm s^{-1} [16] for the surface and inner directions of solid SiO$_2$, respectively. Furthermore, the reaction for the inner direction becomes slower with the electrolysis time because the diffusion length for the O^{2-} ions in the porous Si layer becomes larger. Thus, the larger alloy formation rate than the reduction rates suggests the fast removal of the porous Si layer formed at the outermost surface of the SiO$_2$. This behavior is similar to the removal of Nd–Fe liquid alloy from the surface of iron cathode in the rare earth electrometallurgy [66]. The removal of the surface layer retarding the diffusion of O^{2-} ions would to lead to the continuation of the fast reaction which was confirmed to be equivalent to 0.7 A cm^{-2} in the Hall-Héroult process using molten salt electrolysis [20,21].

Table 3. Thickness of Si plate or diameter of Si rod and alloy formation rate into Zn pool at each Si concentration at 1123 K.

Si conc. in Zn pool, c_{si} / at%	Immersion time, t_{im} / s	Thickness of Si plate			Alloy formation rate [b], v_{alloy} / µm s^{-1}
		Before immersion, L_{bef} / µm	After immersion, L_{aft} / µm	Reduced value for one side [a], $L_{reduced}$ / µm	
0	0	–	–	0	4.56 [c]
	2	534	494	20	
	20	531	378	77	
	40	530	158	186	

	60	526	0	(263)	
1.10	120	4021	3171	425	3.54
2.40	120	5992	5332	330	2.75
4.87	60	530	428	51	0.85

a: $L_{reduced} = \dfrac{L_{bef} - L_{aft}}{2}$

b: $v_{alloy} = \dfrac{L_{reduced}}{t_{im}}$

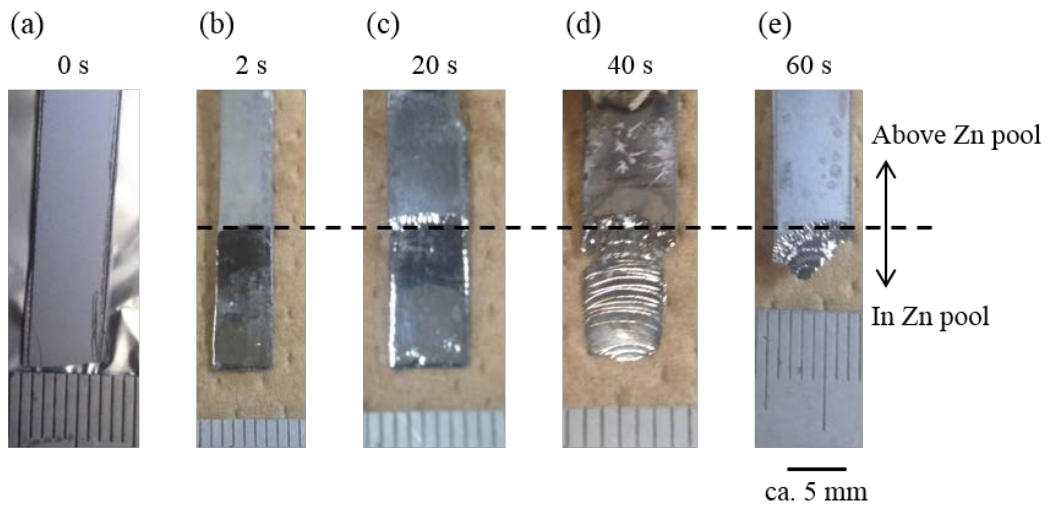c: Calculated from the slope of the plots in Fig. 10.

Figure 9. Photographs of the Si plates (a) before and after the immersion into Zn pool at 1123 K for (b) 2 s, (c) 20 s, (d) 40 s, and (e) 60 s.
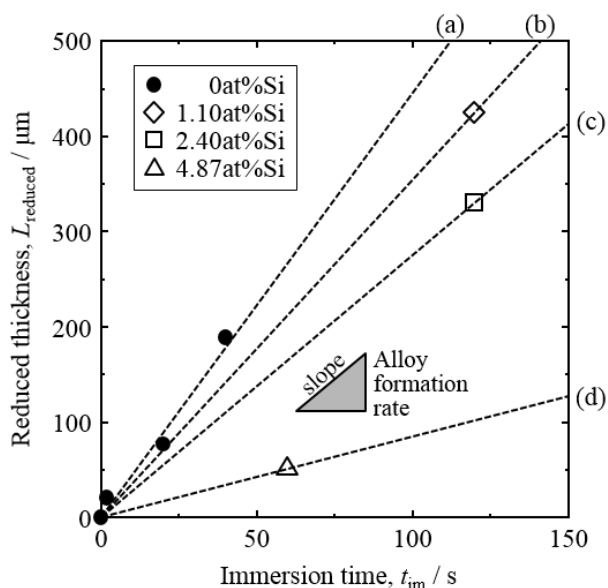
Figure 10. Decreased thickness of Si plate and rod after immersion at 1123 K. Si concentration in Zn pool was (a) 0 at%, (b) 1.10 at%, (c) 2.40 at%, and (d) 4.87 at%.
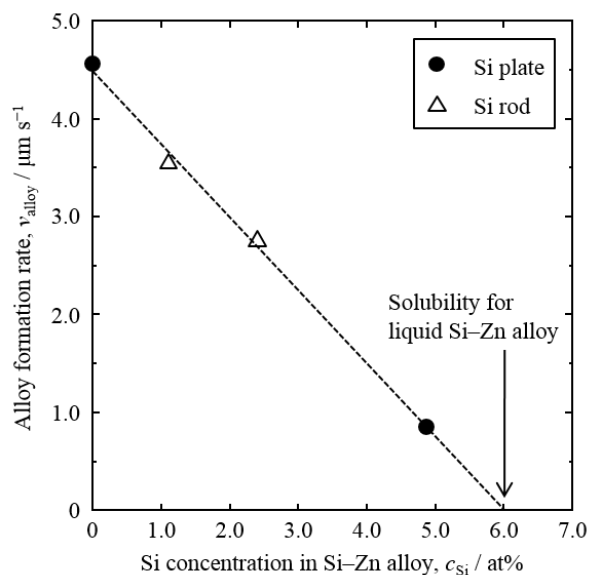

Figure 11. Dependence of alloy formation rate on Si concentration in liquid Si–Zn alloy at 1123 K.

Conclusions

The electrolytic production process of SOG-Si utilizing liquid Si–Zn alloy in molten CaCl$_2$ was proposed. The presence of molten salt above a liquid Zn layer significantly suppressed the evaporation of Zn. The evaporation rate at 1123 K was 0.18 mm day^{-1} ,which is enough small to use as a liquid Zn cathode. The reduction of SiO$_2$ granules on the Zn cathode to form liquid Si–Zn alloy was suggested to proceed from 1.45 V vs. Ca^{2+}/Ca and confirmed at 0.9 V. The alloy formation rate of solid Si and liquid

Zn was measured to be 4.56 μm s^{-1} at 1123 K, which indicates the potential of fast reduction of SiO$_2$.

Acknowledgments

References

1. *Photovoltaic Market 2014*, RTS Corp., Tokyo, Japan, 2014. [in Japanese]
2. *Rare Metal News*, on Aug. 24, 2014, Arumu Publishing Co., Tokyo, Japan. [in Japanese]
3. H. Schweickert, K. Reuschel, and H. Gutsche: U.S. Patent, US3,011,877, 1961.
4. H. Gutsche: U.S. Patent, US3,042,494, 1962.
5. F. Bischoff: U.S. Patent, US3,146,123, 1964.
6. K. Reuschel and A. Kersting: U.S. Patent, US3,200,009, 1965.
7. K. Yasuda and T. H. Okabe: *JOM*, 2010, vol. 62, pp. 94–101.
8. K. Yasuda, K. Morita, and T. H. Okabe: *Energy Technology*, 2014, vol. 2, pp. 141–54.
9. G. Bye and B. Ceccaroli: *Sol. Energy Mater. Sol. Cells*, 2014, vol. 130, pp. 634–46.
10. T. Nohira, K. Yasuda, and Y. Ito: *Nat. Mater.*, 2003, vol. 2, pp. 397–401.
11. K. Yasuda, T. Nohira, K. Amezawa, Y. H. Ogata, and Y. Ito: *J. Electrochem. Soc.*, 2005, vol. 152, pp. D69–74.
12. T. Nohira, *Yoyuen Oyobi Koon Kagaku*, 2011, vol. 54, pp. 95–103. [in Japanese]
13. K. Yasuda, T. Nohira, R. Hagiwara, and Y. H. Ogata: *Electrochim. Acta*, 2007, vol. 53, pp. 106–10.
14. K. Yasuda, T. Nohira, K. Kobayashi, N. Kani, T. Tsuda, and R. Hagiwara: *Energy Technology*, 2013, vol. 1, pp. 245–52.
15. T. Toba, K. Yasuda, T. Nohira, X. Yang, R. Hagiwara, K. Ichitsubo, K. Masuda, and T. Homma: *Electrochemistry*, 2013, vol. 81, pp. 559–65.
16. K. Yasuda, T. Nohira, and Y. Ito: *J. Phys. Chem. Solids*, 2005, vol. 66, pp. 443–47.
17. K. Yasuda, T. Nohira, R. Hagiwara, and Y. H. Ogata: *J. Electrochem. Soc.*, 2007, vol. 154, pp. E95–101.
18. K. Yasuda, T. Nohira, K. Takahashi, R. Hagiwara, and Y. H. Ogata: *J. Electrochem. Soc.*, 2005, vol. 152, pp. D232–37.
19. Y. Nishimura, T. Nohira, K. Yasuda, Y. Fukunaka, and R. Hagiwara: *Trans. Mater. Res. Soc. Jpn.*, 2010, vol. 35, pp. 47–49.
20. X. Yang, K. Yasuda, T. Nohira, R. Hagiwara, and T. Homma: *Metall. Mater. Trans. B*, 2014, vol. 45B, pp. 1337–44.
21. X. Yang, K. Yasuda, T. Nohira, R. Hagiwara, and T. Homma: *J. Electrochem. Soc.*, 2014, vol. 161, pp. D3116–19.

22. X. Yang, K. Yasuda, T. Nohira, R. Hagiwara, and T. Homma: *Metall. Mater. Trans. B*, 2016, vol. 47B, pp. 788–97.
23. X. Jin, P. Gao, D. Wang, X. Hu, and G. Z. Chen: *Angew. Chem.*, 2004, vol. 116, pp. 751–54.
24. P. C. Pistorius and D. J. Fray: *J. S. Afr. Inst. Min. Metall.*, 2006, vol. 106, pp. 31–41.
25. W. Xiao, X. Jin, Y. Deng, D. Wang, X. Hu, and G. Z. Chen: *ChemPhysChem,* 2006, vol. 7, pp. 1750–58.
26. S. Lee, J. Hur, and C. Seo: *J. Ind. Eng. Chem.*, 2008, vol. 14, pp. 651–54.
27. W. Xiao, X. Jin, Y. Deng, D. Wang, X. Hu, and G. Z. Chen: *J. Electroanal. Chem.*, 2010, vol. 639, pp. 130–40.
28. E. Juzeliunas, A. Cox, and D. J. Fray: *Electrochem. Comm.*, 2010, vol. 12, pp. 1270–74.
29. T. Oishi, M. Watanabe, K. Koyama, M. Tanaka, and K. Saegusa: *J. Electrochem. Soc.*, 2011, vol. 158, pp. E93–99
30. E. Ergül, İ. Karakaya, and M. Erdoğan: *J. Alloy. Compd.*, 2011, vol. 509, pp. 899–903.
31. W. Xiao, X. Wang, H. Yin, H. Zhu, X. Mao, and D. Wang: *RSC Advances,* 2012, vol. 2, pp. 7588–93.
32. S. K. Cho, F. F. Fan, and A. J. Bard: *Electrochim. Acta*, 2012, vol. 65, pp. 57–63.
33. S. K. Cho, F. F. Fan, and A. J. Bard: *Angew. Chem.*, 2012, vol. 124, pp. 12912–16.
34. W. Xiao, X. Jin, and G. Z. Chen: *J. Mater. Chem. A.*, 2013, vol. 1, pp. 10243–50.
35. T. Yoshikawa and K. Morita: *Sci. Technol. Adv. Mater.*, 2003, vol. 4, pp. 531–37.
36. T. Yoshikawa and K. Morita: *CAMP-ISIJ*, 2004, vol. 17, p. 875.
37. T. Yoshikawa and K. Morita: *Proc. EPD Congress 2005*, TMS, Warrendale, pp. 549–58, 2005.
38. T. Yoshikawa and K. Morita: *J. Cryst. Growth*, 2009, vol. 311, pp. 776–79.
39. T. Yoshikawa and K. Morita: *JOM*, 2012, vol. 64, pp. 946–51
40. J. M. Juneja and T. K. Mukherjee: *Hydrometallurgy*, 1986, vol. 16, pp. 69–75.
41. A. M. Mitrašinović and T. A. Utigard: *Silicon*, 2009, vol. 1, pp. 239–48.
42. X. Ma, T. Yoshikawa, and K. Morita: *J. Alloy. Compd.*, 2012, vol. 529, pp. 12–16.
43. X. Ma, T. Yoshikawa, and K. Morita: *Sep. Purif. Technol.*, 2014, vol. 125, pp. 264–68.
44. L. Hu, Z. Wang, X. Gong, Z. Guo, and H. Zhang: *Metall. Mater. Trans. B*, 2013, vol. 44B, pp. 828–36.
45. S. Esfahani and M. Barati: *Metals Mater. Int.*, 2011, vol. 17, pp. 823–29.
46. S. Esfahani and M. Barati: *Metals Mater. Int.*, 2011, vol. 17, pp. 1009–15.
47. L. T. Khajavi, K. Morita, T. Yoshikawa, and M. Barati: *Metall. Mater. Trans. B*, 2015, vol. 46B, pp. 615–20.
48. Z. Yin, A. Oliazadeh, S. Esfahani, M. Johnston, and M. Barati: *Can. Metall. Q.*, 2011, vol. 50, pp. 166–72.
49. H. Morito, T. Karahashi, M. Uchikoshi, M. Isshiki, and H. Yamane: *Silicon*, 2012, vol. 4, pp. 121–25.
50. M. W. Jr. Chase, C. A. Davies, J. R. Jr. Downey, D. J. Frurip, R. A. McDonald and A. N. Syverud: *NIST-JANAF Thermochemical Tables, 4th ed., J. Phys. Chem. Ref. Data, Monograph No. 9*, American Chemical Society and the American Institute of Physics for the National Institute of Standards and Technology, New York, USA, 1998.

51. I. Barin, O. Knacke, and O. Kubaschewski: *Thermochemical Properties of Inorganic Substances, Supplement*, Springer-Verlag, Berlin, Germany, 1977.
52. R.W. Olesinski and G. J. Abbaschian: *J. Phase Equilib.*, 1985, vol. 6, pp. 545–48.
53. R.W. Olesinski and G. J. Abbaschian: *J. Phase Equilib.*, 1984, vol. 5, pp. 273–76.
54. R.W. Olesinski and G. J. Abbaschian: *J. Phase Equilib.*, 1984, vol. 5, pp. 271–73.
55. J. L. Murray and A. J. McAlister: *Bulletin of Alloy Phase Diagrams*, 1984, vol. 5, pp. 74–84.
56. T. Yoshikawa and K. Morita: *Yoyuen Oyobi Koon Kagaku*, 2006, vol. 49, pp. 155–63. [in Japanese]
57. F. A. Trumbore: *Bell System Tech. J.*, 1960, vol. 39, pp. 205–33.
58. M. Maeda: *Seisan Kenkyu, Institute of Industrial Science at University of Tokyo*, 1986, vol. 38, pp. 425–33. [in Japanese]
59. G. J. Kipouros and R. A. Sharma: *J. Electrochem. Soc.*, 1990, vol. 137, pp. 3333–38.
60. T. R. Hogness: *J. Am. Chem. Soc.*, 1921, vol. 43, pp. 1621–28.
61. G. J. Janz: *J. Phys. Chem. Ref. Data, vol. 17, Supplement No. 2*, American Chemical Society and the American Institute of Physics for the National Institute of Standards, New York, USA, 1988, p. 23.
62. T. B. Massalski: *Binary Alloy Phase Diagrams*, ASM International, Materials Park, USA, 1996.
63. J. Delcet and J. J. Egan: *Metall. Mater. Trans. B*, 1978, Vol. 9B, pp. 728–29.
64. M. Kato and S. Minowa: *J. ISIJ*, 1966, vol. 52, pp. 32–41.
65. S. Yang, X. Su, J. Wang, F. Yin, N. Y. Tang, Z. Li, and X. Li: *Metall. Mater. Trans. A*, 2011, vol. 42A, pp. 1785–92.
66. G. Adachi: *Rare Metal Binran,* Maruzen Co., Ltd., Tokyo, Japan, 2011. [in Japanese]